Synthesis and Optical Properties of Silver Nanoparticles and Arrays

David D. Evanoff Jr. and George Chumanov*[a]

This Minireview systematically examines optical properties of silver nanoparticles as a function of size. Extinction, scattering, and absorption cross-sections and distance dependence of the local electromagnetic field, as well as the quadrupolar coupling of 2D assemblies of such particles are experimentally measured for a wide range of particle sizes. Such measurements were possible because of the development of a novel synthetic method for the size-controlled synthesis of chemically clean, highly crystalline silver nanoparticles of narrow size distribution. The method and its unique advantages are compared to other methods for synthesis of metal nanoparticles. Synthesis and properties of nanocomposite materials using these and other nanoparticles are also described. Important highlights in the history of the field of metal nanoparticles as well as an examination of the basic principles of plasmon resonances are included.

1. Introduction

The field of nanoscience has blossomed over the last twenty years and the need for nanotechnology will only increase as miniaturization becomes more important in areas such as computing, sensors, and biomedical applications. Advances in this field largely depend on the ability to synthesize nanoparticles of various materials, sizes, and shapes, as well as to efficiently assemble them into complex architectures. The synthesis of nanoparticles, however, is a fairly established field as particles of submicron or nanosized dimensions have been synthesized for centuries. The first example of considerable recognition is the Roman Lycurgus Cup, a bronze cup lined with colored glass that dates to the fourth Century AD. The glass scatters a dull green light and transmits red light. According to a study commissioned by the British Museum, who currently displays the cup, the glass contains 70 nm particles that are an alloy of silver (70%) and gold (30%).[1] Silver nanoparticles of this size are known to scatter green light and transmit orange, and the addition of Au shifts the absorption band to longer wavelengths. Although this particular application of nanoparticles may have been unintentional, small nanoparticles were often used in later centuries to create stained glass with small, ruby-red Au and lemon-yellow Ag particles.

The first notable scientific study of the optical properties of metal nanoparticle colloidal suspensions and ultrathin metal films was conducted by Michael Faraday in the 1850s.[2] Inspired by the ability of extremely thin Au leaf to transmit green light, Faraday supposed that a material that is capable of strong interaction with light can do so even when its dimensions became smaller than visible wavelengths. He synthesized the characteristic ruby-red Au particle suspensions through a number of methods and showed that while the suspensions reacted to acids in the same way as bulk Au, the particles were apparently too small to be resolved by his microscope. Faraday also demonstrated that the color of Au colloids would predictably change when varying amounts of aggregation-inducing agents were added, and currently many scientists are successfully pursuing these so-called aggregation assays.[3] As a testament to their stability, some of the colloidal suspensions synthesized in Faraday's studies are still on display at London's Royal Institute.

The next significant achievement came in 1908 from Gustav Mie who published his now seminal work on the extinction of light by metal spheres.[4] Kerker, in his excellent historical discussion, however, points out that several scientists prior to Mie published similar studies that remain obscure to the modern scientific community.[5] Mie, who held the title Professor Extraordinarius at the University of Greifswald, initiated experimental investigations of colloidal Au by convincing Walter Steubing to make the study his doctoral thesis.[6] Mie's intent for his 1908 paper was to describe mathematically the optical responses of Au suspensions that Steubing, as well as other scientists such as Faraday and Zsigmondy, had measured.[7] Starting from the macroscopic Maxell equations, Mie calculated the extinction, scattering, and absorption cross-sections of Au nanoparticles and showed how the spectra of the suspensions evolve as a function of particle size. The results of these calculations also allowed him to sketch scattering diagrams for different particle sizes and diagrams depicting the electric and magnetic fields of the dipole, quadrupole, octupole, and sextupole components of the resonance. Now, it is well known that the optical resonances in noble-metal nanoparticles are the collective oscillations of conduction electrons termed plasmons. It is interesting to note how precisely Mie's calculations describe these resonances when considering that the concept of an electron was still a few years from being conclusively proven by Milliken.[8]

The early methods to produce suspensions of very small noble-metal particles are still used today and continue to be the standard by which other synthesis methods are compared.

[a] *D. D. Evanoff Jr., Prof. G. Chumanov*
Department of Chemistry, Clemson University
Clemson, SC, 29634 (USA)
Fax: (+1) 864-656-0567
E-mail: gchumak@Clemson.edu

 DOI: 10.1002/cphc.200500113

The most popular method to produce Au suspensions is the so-called Turkevich method, which employs the reduction of chloroauric acid with sodium citrate and produces a narrow size distribution of $\approx$10 nm particles.[9] Faraday described several methods in his 1857 lecture, although the reduction of gold chloride by phosphorous in carbon disulfide seemed to produce the most highly colored "ruby-red fluids".[2] For Ag nanoparticle suspensions, a common method is the Lee–Meisel method, which is a variation of the Turkevich method in that $AgNO_3$ is used as the metal source,[10] but unlike the Turkevich method, the Lee–Meisel method produces a broad distribution of particle sizes. The most common method for the synthesis of nanosized Ag particles is the reduction of $AgNO_3$ with $NaBH_4$. Referred to as the Creighton method, the synthesis procedure routinely yields $\approx$10 nm particles of narrow size distribution.[11] This method can also be adapted to produce particles of other metals such as Pt, Pd, Cu, Ni, etc.,[12] although the specific protocols depend on the reduction potential of the source ion. Cu and Ni suspensions, for example, are not very stable as the metal particles are easily oxidized requiring strong capping ligands to prevent the oxidation.

2. Silver Nanoparticle Synthesis

Of the three metals (Ag, Au, Cu) that display plasmon resonances in the visible spectrum, Ag exhibits the highest efficiency of plasmon excitation.[13a] Moreover, optical excitation of plasmon resonances in nanosized Ag particles is the most efficient mechanism by which light interacts with matter. A single Ag nanoparticle interacts with light more efficiently than a particle of the same dimension composed of any known organic or inorganic chromophore. The light-interaction cross-section for Ag can be about ten times that of the geometric cross-section, which indicates that the particles capture much more light than is physically incident on them.[14] Silver is also the only material whose plasmon resonance can be tuned to any wavelength in the visible spectrum.

Numerous methods for the synthesis of Ag nanoparticles have been reported in the literature and can be arbitrarily divided into *traditional* and *non-traditional* categories. *Traditional* are those solution-phase synthesis techniques that are based on various modifications of the Lee–Meisel or Creighton methods described above, and there are a host of examples in which different Ag salts and reducing agents are used.[15] Due to the large positive reduction potential of Ag, nanoparticle oxidation is thermodynamically unfavorable resulting in quite stable aqueous and alcoholic suspensions without the aid of capping ligands. Aggregation can be inhibited by the thick electrical double layers that form around metal nanoparticles in low-ionic-strength suspensions. For high ionic strengths or organic-phase suspensions, capping agents such as self-assembled monolayers,[15c,e] surfactants,[15a–b,16] polymers,[15g,i-k] and dendrimers[17] can be employed to protect the particles from aggregation. If the synthesis is carried out in the presence of capping agents, however, anisotropic particles may result due to the differing affinities of the ligands to the exposed crystal faces. This is sometimes a desired effect and several researchers have shown that various shapes can be produced through judicious use of stabilizing agents.[16,18] Alternatively, nanoparticles can be capped with desired molecules after the synthesis to facilitate their transfer into nonpolar phases or to tailor their surface chemistry. *Non-traditional* synthesis methods include Ag particle synthesis through high-temperature reduction in porous solid matrices,[19] vapor-phase condensation of a metal onto a solid support,[20] laser ablation of a metal target into a suspending liquid,[21] photoreduction of Ag ions,[22] and electrolysis of an Ag salt solution.[23]

The above discussion is by no means a complete listing of the available synthetic methods, but rather a broad sampling of what has been reported. Unfortunately, all of the methods listed have some inherent problems, and while each method has certain advantages and disadvantages, the selection of a proper synthetic procedure depends on the nature of the nanoparticle application. With the traditional methods, the major problem is often a limited flexibility in the size of particles that can be produced and such methods are usually sold on their ability to make $<$10 nm particles. Certainly, small particles are desirable in catalysis, where the main emphasis is on surface-to-volume ratio, but for optical applications, larger particles are often necessary. Small Ag nanoparticles do not interact with light nearly as efficiently as particles that are in the 50–100 nm range and do so strictly through energy absorption. On the other hand, the plasmon resonances in larger Ag nanoparticles have a significant light-scattering component that can be advantageously used in applications that require efficient optical labels, such as in chemical assays. The major problems for the *non-traditional* methods are often a wide size distribution, lack of particle crystallinity, and the cost and scalability of the production. The optimum synthetic method should address all of the above problems and additionally yield particles with no extraneous chemicals that can potentially alter the particle's optical properties and surface chemistry.

A synthetic method that fulfills all of the above requirements was developed in our laboratory and involves the reduction of a supersaturated Ag_2O solution at 70 °C by hydrogen gas pressurized at 10 psi above atmosphere. During the synthesis reaction, silver ions are slowly supplied to the growing particles due to the limited solubility of Ag_2O (ca. 50 mg L^{-1}).[24] This slow-growth approach is different from the traditional methods, in which the entire metal-ion supply is available at the beginning of the reduction process. As the reaction proceeds, the concentrations of both the metal ions and the reducing agent deplete, changing the particle growth kinetics, leading to broad size distributions. In the current approach, however, the concentration of silver ions and H_2 remain constant for the entire reaction, resulting in particles of higher crystallinity and a more narrow size distribution. The particle size can readily be controlled in the range of ten to above 200 nm,[25] with the standard deviation of particle size consistently between 5% and 8%, simply by varying the reaction time. The Ag suspensions are quite pure as the only species present in the reaction are Ag, hydrogen, and water, and high-purity reactants are commercially available. Particle stability is achieved through electrostatic repulsion between the

thick electrical double layers that result from the limited dissociation of Ag oxide. The typical concentrations of Ag nanoparticle suspensions synthesized by this method are around 10^{10} cm^{-3}, but can be further concentrated to 10^{12}–10^{13} cm^{-3}. The size and shape distributions of the particle suspensions commonly synthesized by hydrogen reduction are depicted in Figure 1.

3. Nanocomposite Synthetic Methods

The incorporation of nanoparticles into various matrices will extend their utility in material and device applications. Such nanocomposites could exhibit novel optical properties as the plasmon resonances are strongly affected by the surrounding matrix as well as because closely spaced particles in matrices can exhibit cooperative phenomena when interacting with light.

Our work is focused on coating of nanoparticles with metal-oxide and polymer layers and their incorporation into matrices of such materials. Coatings are used to protect the particles from aggressive environments and to introduce chemical functionality to their surface. Previously, Liz-Marzán et al. reported the coating of Au nanoparticles by amorphous silica using sol-gel chemistry.[26] This is a modification of the well-known Stöber approach used to synthesize nano- or micron-sized silica particles via acid or base hydrolysis of silicon alkoxide followed by spontaneous condensation.[27] Here, this approach was extended to coat H_2 reduced Ag nanoparticles with silica, titania, and tungstate, in which the metal particles act as condensation centers and careful control of the metal/alkoxide ratio can completely inhibit spontaneous condensation of the free precursor. The resulting shell thickness was uniform among particles and could reproducibly be varied between 7 and 60 nm. The lower limit is determined by the thickness at which the condensation forms a uniform shell as opposed to individual islands. Beyond 60 nm, the required alkoxide concentration induces spontaneous condensation, which results in the formation of free oxide particles.[28] A few examples of the silica-coated Ag particles are shown in Figure 2. The use of silica protection of Ag nanoparticles is beneficial for biochemical applications as molecules such as DNA, proteins, etc. will react with the particles via chemical groups that exhibit affinity to Ag. In addition, protocols for the immobilization of these molecules to glass are well developed.

Titania is an especially interesting oxide as its crystalline forms, rutile and anatase, are widely used as a photocatalyst and in photovoltaic applications. Titania is a wide-bandgap indirect semiconductor, in which excitation with light larger than 3.2 eV (388 nm) generates long-lived electron–hole pairs. However, for the efficient conversion of solar radiation (λ_{max} ca. 480 nm) into electrical or chemical energy, the bandgap of TiO_2 must be shifted to longer wavelengths. Such sensitization is usually achieved with organic dye molecules that absorb in the visible spectral range to better match with the solar spectrum. The addition of Ag nanoparticles to this system can further increase the excitation efficiency of the dye or can possibly act as the sensitizer itself through the coupling of the plasmon resonance in Ag nanoparticles to the electron–hole-pair generation in titania. The incorporation of Ag nanoparticles into a titania matrix can also be useful for modulating the frequency of plasmon modes in Ag nanoparticles and their assemblies via the high refractive index of TiO_2. Recently, it was demonstrated that the coating of Ag nanoparticles with amorphous titania layers of varying thickness can be accomplished

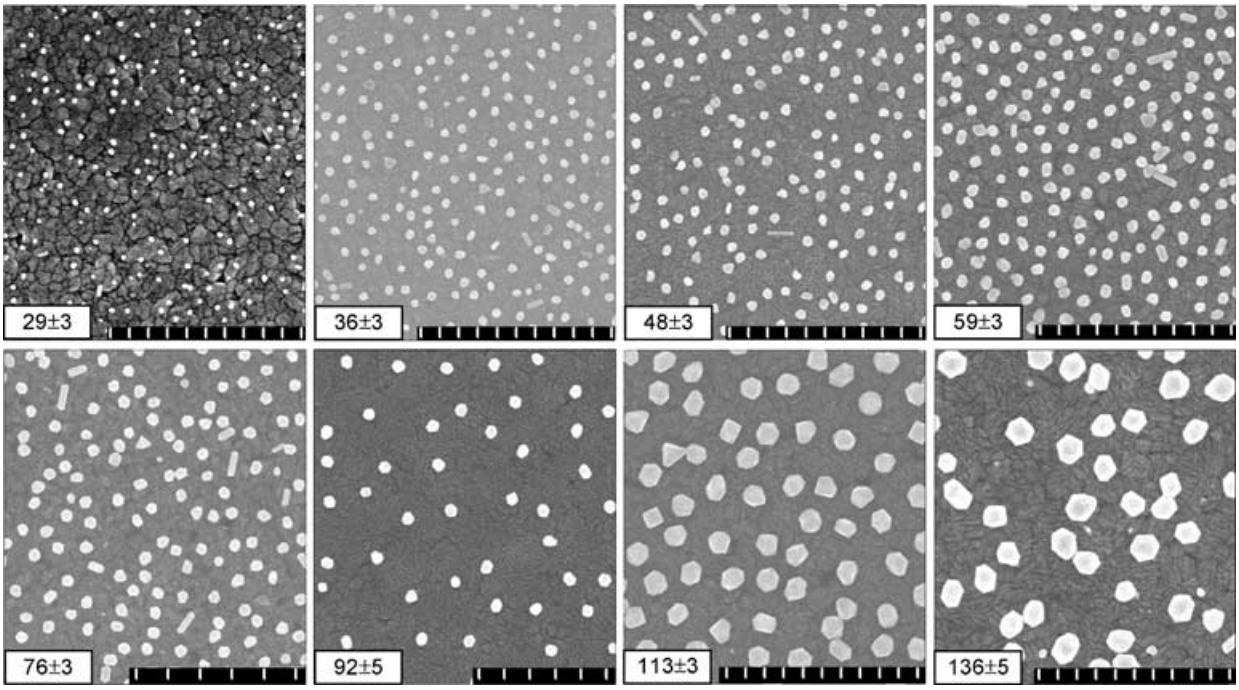

Figure 1. SEM images of different sizes of silver nanoparticles synthesized by hydrogen reduction. Mean particle diameters and 1 μm scale bars are shown in each panel.

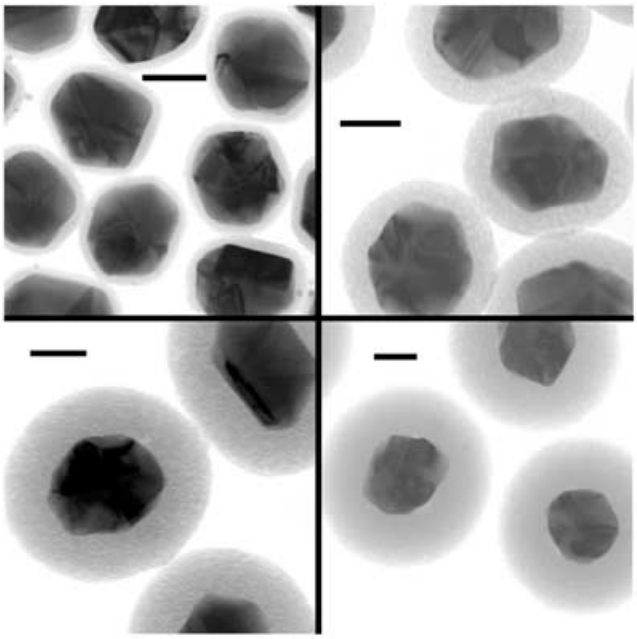

Figure 2. STEM images of silica coatings of various thicknesses. The scale bar in each panel is 50 nm.

with sol-gel chemistry. Hydrothermal treatment of these particles led to conversion of the amorphous titania into the anatase form. Coatings with both the amorphous and anatase forms of TiO_2 are shown in Figure 3.[29]

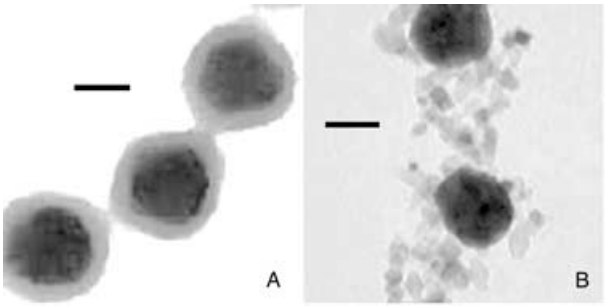

Figure 3. TEM images of the A) amorphous and B) anatase forms of titania around silver nanoparticles. The scale bar in each panel is 50 nm.

Another interesting material is the electrochromic tungsten oxide (WO_3), which exhibits a reversible redox chemistry to form a reduced tungsten oxide, that is, tungsten bronze, of mixed valency, M_xWO_3, where M_x ($0 < x < 1$) indicates the insertion of cation.[30] The reduced and oxidized forms have different conductivities and exhibit different colors. While WO_3 is transparent and has low conductivity, the color of M_xWO_3 varies between deep blue with n-type semiconductor characteristics ($x \approx 0.3$) to bronze with semimetallic properties ($x \approx 0.9$). Monolayers of Ag nanoparticle were adsorbed on transparent conducting electrodes and sol-gel chemistry was utilized to deposit WO_3 around and on top of the particles. By sweeping the electrochemical potential of these nanocomposite electrodes, the plasmon resonance was rapidly modulated (Figure 4). Variations in the intensity and position of the plasmon resonance was interpreted as due to changes in the refractive index of the medium surrounding the particles as the potential is cycled between the two forms of tungsten oxide. In this way, a simple plasmon-based electro-optical device was demonstrated.[31] With the same tungsten peroxyester precursor employed in the above experiment, Ag particles were also coated with WO_3 in suspension using a similar protocol as that for silica and titania and resulting in similar shell thicknesses and uniformity.

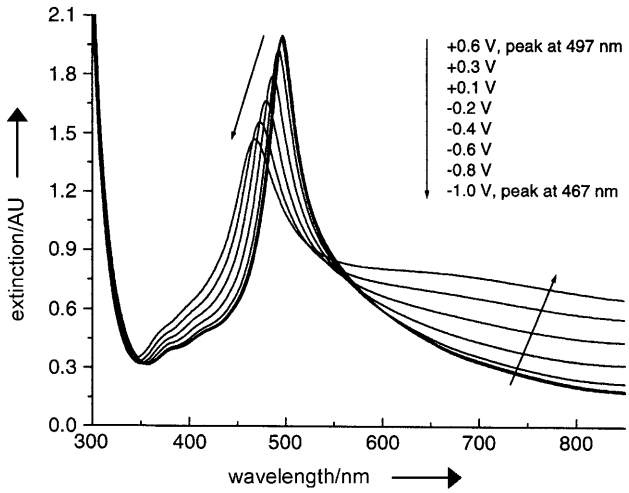

Figure 4. UV/Vis extinction spectra of a silver/tungsten oxide composite film under different applied potentials. Reproduced with permission from ref. [31].

In addition to oxides, Ag nanoparticles can be coated or embedded into organic polymeric matrices such as poly(dimethylsiloxane),[32] poly(4-vinylpyridine),[33] polystyrene, polymethacrylate,[34] and, most recently, Teflon AF.[35] The main motivation for using organic coatings around nanoparticles is to tailor their surface chemical properties to particular applications and to protect them from chemically aggressive environments. The coating of Ag particles with polystyrene and methacrylate was achieved by emulsion polymerization[34] and resulted in non-aggregated particles with a 2–10 nm polymer coating (Figure 5). Unlike the porous metal-oxide layers synthesized by sol-gel chemistry, the polymer layer can be made sufficiently dense rendering the particles highly resistant to etching in the presence of oxygen. As an example, the exposure of polystyrene-coated Ag nanoparticles to high concentrations of aqueous NaCl did not have an appreciable effect on the plasmon resonance, whereas unprotected particles undergo instantaneous aggregation followed by Cl^- etching as is evident from drastic degradation of the plasmon resonance (Figure 6). The resistance to Cl^- and the ability of the polymer to be further modified by proteins and other biological molecules makes these composite nanoparticles valuable for bioanalytical applications, in which the particles can be used as optical labels.

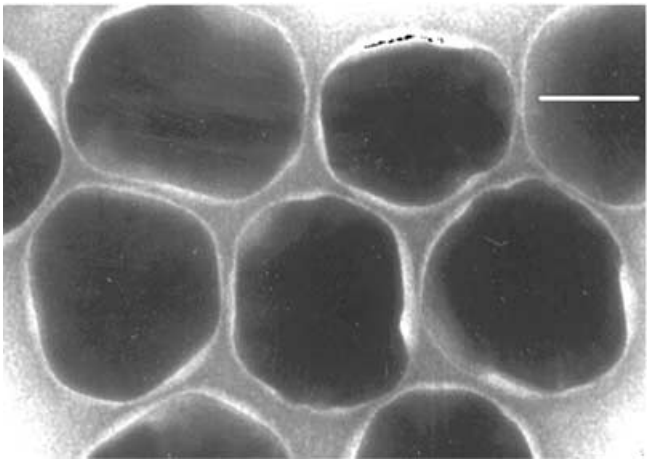

Figure 5. TEM image of silver nanoparticles coated with polystyrene/methacrylate visualized through negative staining with phosphotungstic acid. The scale bar is 50 nm.

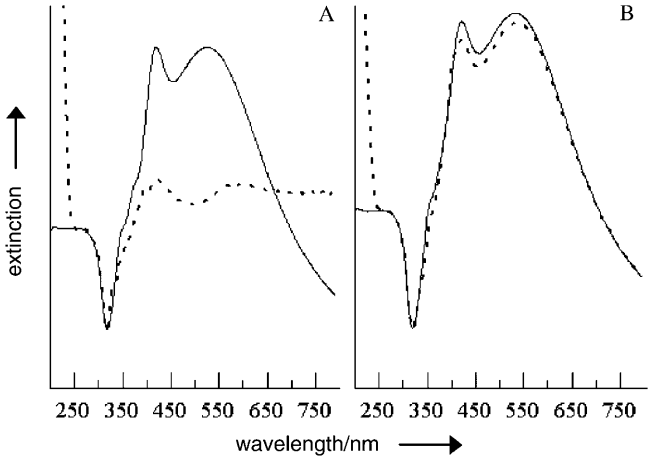

Figure 6. UV/Vis extinction spectra of A) uncoated and B) polystyrene-coated silver nanoparticles in water (——) and 1.8 M NaCl (-----).

Teflon AF is an exceptional polymer in that it has a refractive index less than that of water and the lowest dielectric constant of any plastic.[36] The amorphous nature of this fluorinated copolymer and its solubility in a number of fluorinated solvents allow the casting of films that are transparent from the IR to deep UV spectral range. Because of these optical properties, as well as the chemical inertness of Teflon AF, its use in several advanced applications is currently being explored.[37] Incorporation of various metal nanoparticles into a Teflon AF matrix will yield nanocomposite materials with novel, practically important properties for photonic devices, as well as for catalysis in high-pH environments. Unique solution-phase synthesis techniques were recently developed for the doping of Teflon AF with metal nanoparticles.[35b] The only other reported method to produce such nanocomposites involves the vacuum codeposition of the metal and the fluoropolymer.[38] The solution-based methods are: 1) the direct synthesis of metal nanoparticles in a Teflon AF solution and 2) the phase transfer of previously synthesized particles into the polymer solution. The direct synthesis relies on the judicious use of a class of fluorinated metal acetylacetonates that allows the synthesis of nanoparticles from a wide variety of metals and metal oxides. Both methods utilize a fluorinated solvent, decafluoropentane, which both solubilizes Teflon AF and mixes with metal salt solutions and nanoparticle suspensions in low alcohols. The direct synthesis allows rapid preparation of large quantities of nanocomposites and is the preferred method for metal particles that are easily oxidized. This method, however, leads to fairly wide particle size and shape distributions because Ostwald ripening is inhibited. The phase-transfer method is the better choice if careful regulation of particle size and shape is important because the distributions can be independently controlled in a separate reaction. Either method results in high-metal-content composite materials that can be dispersed in fluorinated solvents and cast into films and templates for device fabrication. Electron micrographs of the Teflon AF nanocomposites synthesized by the direct method and containing four different metals are shown in Figure 7.

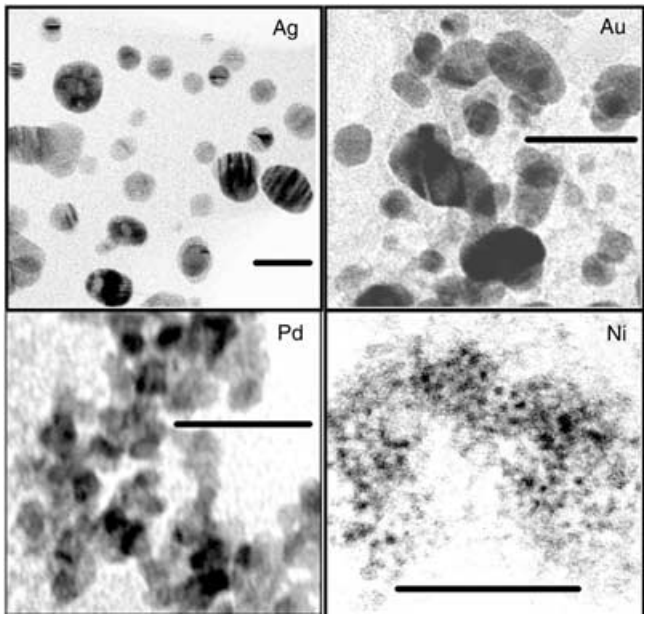

Figure 7. STEM images of Teflon AF matrices doped with different metals. The scale bar in each panel is 30 nm.

4. Optical Properties of Silver Nanoparticles

4.1. Plasmon Resonances of Metal Nanoparticles

The unique optical properties of metal nanoparticles originate from the collective oscillations of conduction electrons, which, when excited by electromagnetic (EM) radiation, are termed surface plasmon polariton resonances (SPPR).[13b] The factors that collectively lead to these oscillations are: 1) acceleration of the conduction electrons by the electric field of incident radiation, 2) presence of restoring forces that result from the induced polarization in both the particle and surrounding medium, and 3) confinement of the electrons to dimensions smaller than the wavelength of light. The electric field of the

incident EM radiation displaces the particle's electrons from equilibrium and, in turn, produces a restoring force that results in oscillatory motion of the electrons with a characteristic frequency, that is, the SPPR frequency. At the same time, the oscillating electrons induce polarization of the opposite direction in the surrounding medium, and this polarization reduces the restoring force for the electrons thereby shifting the SPPR to a lower frequency. By controlling the dielectric constant of the surrounding medium, the wavelength of the SPPR can be fine-tuned to a desired position, as is shown in Figure 8. In the first panel, the SPPR is shifted to shorter wavelengths due to the decrease in the dielectric constant from that of isopropanol to that of Teflon AF.[35] In the last two panels, the dielectric constant of the surrounding medium is increased from that of water to that of silica[28] and titania,[29] respectively, red-shifting the SPPR wavelength. SPPR-wavelength modulation via dielectric environment can be used in chemical assays in which varying the concentration of an analyte causes a predictable wavelength shift.[39] The shape of the SPPR spectrum is determined by the relative dimensions of the particle to that of the wavelength of incident EM radiation. For nanoparticles much smaller than the wavelength of light, the EM field is uniform across a particle such that all the conduction electrons move in-phase producing only dipole-type oscillations (Figure 9A) manifested by a single, narrow peak in the SPPR spectrum. As the size increases, the field across the particle becomes nonuniform, and this phase retardation broadens the dipole resonance and excites higher multipole resonances, such as the quadrupole, octupole, etc. (Figures 9B and 9C) leading to several peaks in the spectra.[40] In Figure 10, the SPPR extinction spectra of Ag suspensions of different particle diameters are shown. It is apparent that the dipole maximum rapidly shifts to longer wavelengths as the particle size increases beyond 70 nm (450 nm spectral maximum) revealing the quadrupole peak at about 420 nm. The observed spectral shift results from the "spreading" of the particle's surface charge over a larger surface area so that the surrounding medium better compensates the restoring force thus slowing the electron oscillations.[13c]

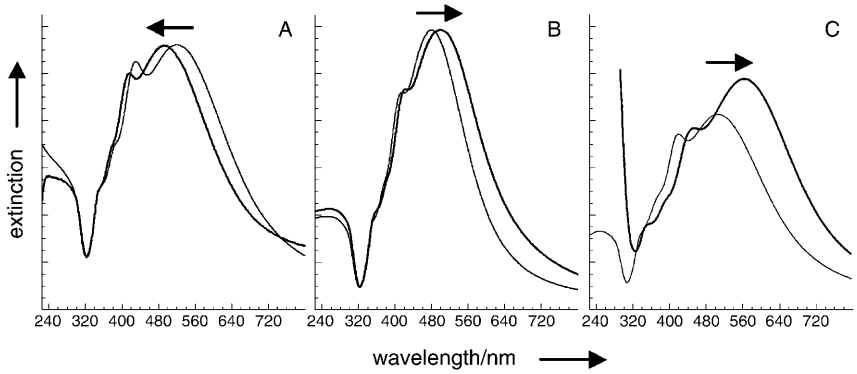

Figure 8. UV/Vis extinction spectra of silver nanoparticle suspensions before (——) and after (——) changes were made to the dielectric environment from A) isopropanol to Teflon AF, B) water to silica, and C) water to titania.

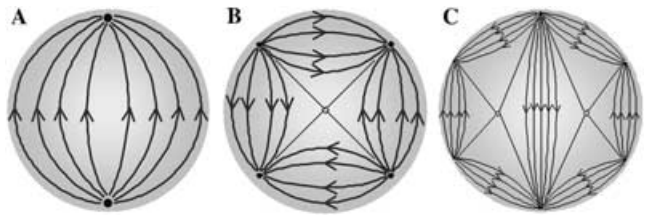

Figure 9. Diagrams depicting the electric field lines of the A) dipole, B) quadrupole, and C) octupole resonances, after ref. [4].

A sufficiently small particle of any conducting material exhibits SPPRs, yet its spectral position depends on many factors, most importantly on the material's frequency-dependent complex dielectric function. The wavelength dependence of the real ($\varepsilon_1(\omega)$) and imaginary ($\varepsilon_2(\omega)$) parts of the dielectric function describing polarizability and energy dissipation, respectively, are given in Figure 11 for Ag.[41] An SPPR occurs when there is phase-matching between the polarization in the particle and incident field, a condition that is fulfilled for very small particles (<10 nm) when $\varepsilon_1(\omega) = -2\varepsilon_m$, where ε_m is the dielectric constant of the surrounding medium,[42] and is satisfied for very small Ag particles suspended in water ($\varepsilon_m = 1.77$) at an excitation wavelength of around 385 nm. The imaginary part of the metal dielectric function, which describes losses, must be small at the SPPR frequency to provide efficient electron oscil-

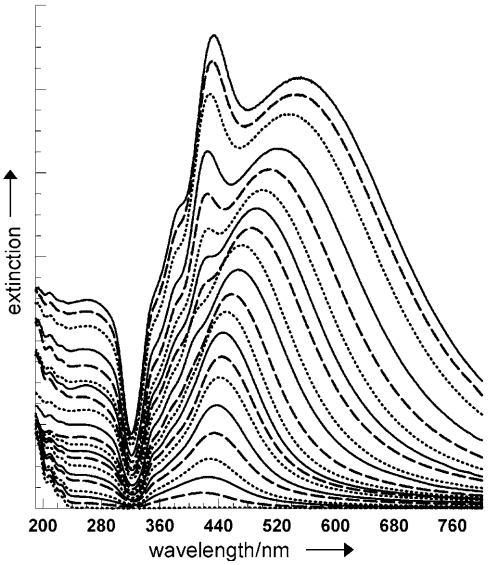

Figure 10. UV/Vis extinction spectra of silver nanoparticle suspensions of 20 different particle diameters.

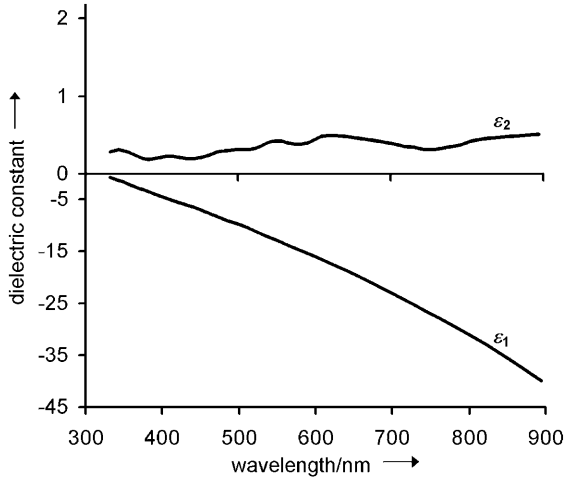

Figure 11. Real and imaginary parts of the dielectric function of silver as a function of wavelength. Curves were prepared using values listed in ref. [41].

lations. Several processes can damp the oscillations, such as electron scattering by lattice phonon modes, inelastic electron–electron interactions, scattering of the electrons at the particle surface, and excitation of bound electrons into the conduction band (interband transitions).[43, 13d] Whereas electron–phonon interactions account for a majority of $\varepsilon_2(\omega)$, inelastic electron–electron interactions and surface scattering are less significant, with the latter being important only for <5 nm particles. Interband transitions can cause a substantially decreased efficiency of plasmon excitation, as is the case for Au and Cu, where there is significant overlap between the interband absorption edge and the plasmon resonance. For Ag, however, the absorption edge is in the UV (ca. 320 nm)[13e] and has little impact on the SPPRs, which appear at wavelengths larger than 370 nm, accounting for the fact that excitation of the SPPR in Ag particles is more efficient than for Au and Cu.

4.2. Absorption and Scattering by Silver Nanoparticles

Once excited, plasmon oscillations can be damped non-radiatively by absorption caused by electron–phonon interactions, and/or radiatively by the resonant scattering process. Plasmon absorption is the only process in small particles, whereas both absorption and scattering are present in large Ag particles, with the latter becoming more dominant as particle size increases. Absorption can cause a fairly drastic temperature change in the particles when high-energy, pulsed laser excitation is used such that breathing modes of the particle lattice are excited, which can be seen as very small Stokes-shifted peaks (8–15 cm^{-1}) in the Raman spectra.[44]

The relative contributions from radiative damping through resonant scattering and absorption strongly depend on the particle size. The contributions of absorption and resonant scattering to extinction with respect to particle size are shown in Figure 12. Whereas particles smaller than 30 nm exhibit only absorption, light extinction of particles larger than about 50 nm is dominated by resonant scattering. At 50 nm, both the absorption and scattering become equal but their spectral maxima are shifted relative to each other.[14a]

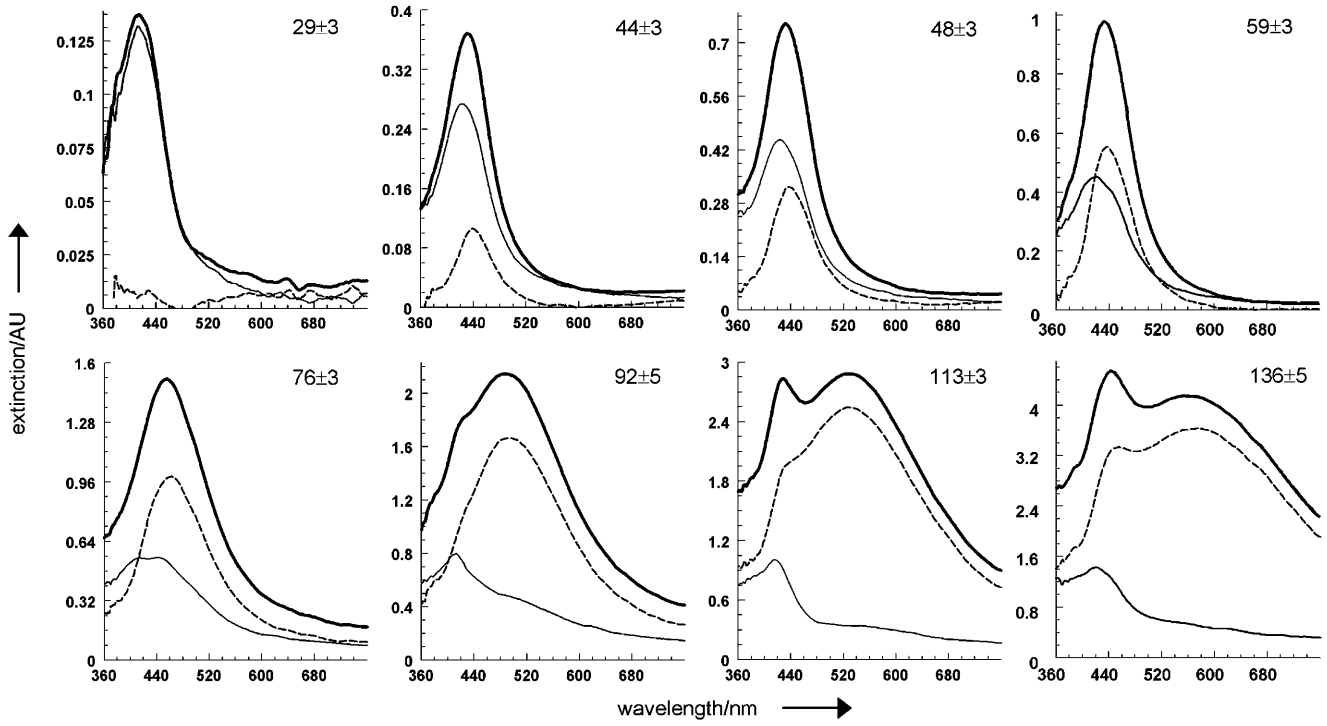

Figure 12. Extinction (——), scattering (-----), and absorption (——) spectra of silver nanoparticle suspensions normalized per particle. The mean particle sizes are noted in each panel. The units on the *y* axis are multiplied by 10^{10}.

The absorption at the SPPR is a property of the metal itself, specifically $\varepsilon_2(\omega)$, whereas scattering is related to the $\varepsilon_1(\omega)$ contribution. Whether the SPPR is absorbing or scattering depends on the magnitude of real and imaginary parts of the dielectric function at the resonance frequency. As can be seen in Figure 11, $\varepsilon_2(\omega)$ is relatively frequency-independent through the visible spectral range while $|\varepsilon_1(\omega)|$ rapidly increases with wavelength. Because $\varepsilon_2(\omega)$ is nearly constant in this spectral range, one would expect the absorption to increase with the geometric cross-section. However, as $|\varepsilon_1(\omega)|$ increases at longer wavelengths, the scattering also increases and competes with the absorption. As a result, the absorption does not increase appreciably, and the increase in extinction at the SPPR frequency for large particles is solely due to the increase in scattering. Extinction is dominated by scattering simply because it is a faster process, resulting from free-electron oscillations, as compared to the slower absorption process that requires interactions with lattice phonons. It was reported that damping due to absorption processes occurs on the time scale of about 40 fs[45a,13d,43] whereas radiative damping can occur on the order of 10 fs.[45b,c] This competition between absorption and scattering can clearly be followed in Figure 12. At a particle size larger than about 50 nm, both dipole and quadrupole resonances contribute to absorption, and the contributions become nearly equal for 75 nm particles. As the size increases further, the contribution from the dipole absorption becomes progressively less important, due to the competition from dipole scattering, and the maximum of the absorption remains at the quadrupole resonance.

4.3. Silver Nanoparticle Extinction, Scattering, and Absorption Cross-Sections

Light that is extinguished by an object is quantified as the extinction cross-section (C_{ext}), which for Ag nanoparticles is larger than the particle's geometric cross-section. This nontrivial fact, which indicates that a particle interacts with light both directly impinging on it and passing within close proximity, can be understood by assuming the following intuitive model. Generally, collisions between two objects depend on their geometric cross-sections and, if one of the objects is much smaller than the other one, the interaction is dominated by the geometric cross-section of the larger object. The photon can be assumed to have a "geometric cross-section" related to its wavelength that is considerably larger than the particle size, thereby providing a possibility for C_{ext} to be larger than the geometric cross-section of the particle. Whether or not this possibility is realized also depends on the rate at which a particle can dissipate energy from the field. In the case of Ag nanoparticles, efficient energy dissipation is achieved through the absorption and scattering of light via excitation of SPPRs. For individual molecules, on the other hand, the ability to dissipate energy is exceedingly low, such that C_{ext} is always much smaller than the geometric cross-sections of both the photon and the molecule.

The extinction efficiency is calculated as the ratio of the extinction cross-section to the geometric cross-section. For Ag, it varies between three and ten depending on the particle diameter. Using the absorption and scattering components of the extinction spectrum, absorption (C_{abs}) and scattering (C_{sca}) cross-sections, as well as efficiencies, can be described in a similar manner. For separate determination of C_{ext}, C_{abs}, and C_{sca}, a scattering spectrometer was constructed and a method was developed for the measurement of the particle concentration. The method, which is described elsewhere, is termed standard subtraction and involves the measure of the extinction spectra prior and after the removal of a precisely known number of particles from the suspension.[14a] The particles are removed by exposing an amine-modified substrate to the suspension,[33] counted using scanning electron (SEM) micrographs, and the cross-sections are determined from measured differences in the extinction. The corresponding efficiencies for various particle diameters are shown in Figure 13. Because cross-sections

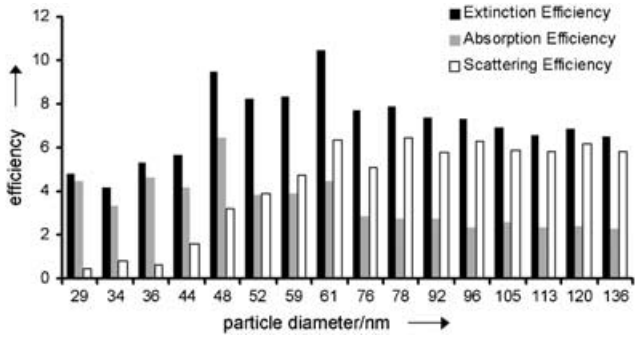

Figure 13. Extinction, scattering, and absorption efficiencies as a function of particle size.

are commonly calculated based on spectral maxima, the extinction and scattering efficiencies reported here are for the dipole resonance maximum, while the absorption efficiency represents the absorption maximum that is at the dipole, quadrupole or a mixture of both resonances, depending on the particle size.[14a]

Relationships of absorption and scattering cross-sections to particle size and the position of the SPPR maximum are shown in Figure 14. C_{abs} increases linearly with the geometric cross-section in the spectral region in which scattering is unimportant because the absorption mechanism due to the electron–phonon interactions is the same, regardless of particle size (Figure 14A). For this reason, plasmon absorption can be thought of as a property not of the SPPR but of the metal itself. On the contrary, C_{sca} appears to increase linearly with the particle volume rather than with its geometric cross-section (Figure 14B). This relationship indicates that scattering depends on the total number of conduction electrons participating in the oscillation and thus is a property of the resonance.

4.4. Extension of the Local Field from the Silver Nanoparticle Surface

When SPPRs are excited, the oscillating electrons generate an EM field consisting of two components: a local non-radiative

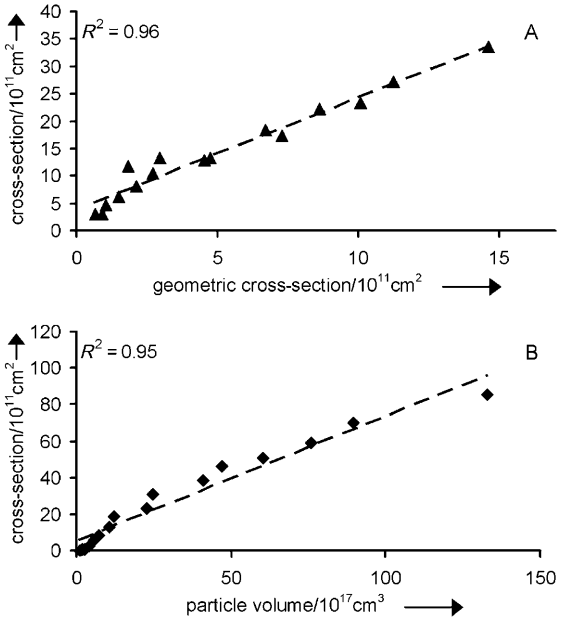

Figure 14. Graphs illustrating the linear relationships between A) absorption cross-section and geometric cross-section and B) scattering cross-section and particle volume.

field around the particles that is enhanced as compared to the incident field and a radiative EM field due to resonant scattering.[46] The distance to which the local field extends from the particle surface plays a major role in various surface-enhanced phenomena as molecules placed within this field experience increased induced polarization.[47] At the same time, the molecules perturb the field by affecting the local dielectric environment and, because the oscillating electrons and the local field are inseparable parts of the same system, alter the frequency of electron oscillations. Although this model may appear somewhat different from the notion of the restoring force previously introduced to explain the effect of dielectric medium on the frequency of SPPR, it describes the same physical processes.

The distance to which the local field extends from the particle surface was determined by measuring the SPPR wavelength as a function of the thickness of a homogeneous silica layer around the Ag nanoparticles. As the thickness of the silica layer was increased, the wavelength of the resonance shifted to the red due to an increase in the local dielectric constant. After reaching a limiting thickness, further increases in the thickness of the silica layer did not have an effect on the SPPR (Figure 15), and this limiting thickness was attributed to the maximum distance to which the local field extends from the surface of the particles.[28] In a similar fashion, Haes et al. reported similar results using an ideologically similar technique in which multilayers of long-chain thiols were used to control local polarizability.[48]

4.5. Quadrupolar Coupling of 2D Silver Nanoparticle Arrays

The assembly of metal nanoparticles into 1-, 2-, and 3D structures has generated significant interest in the last several years

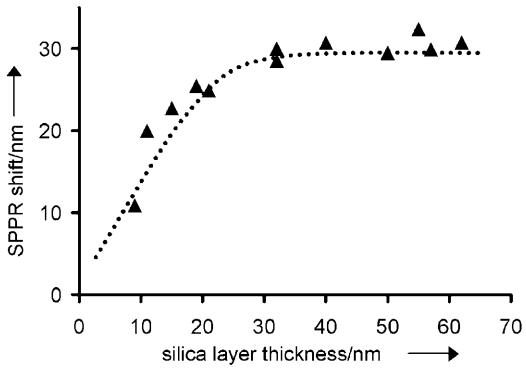

Figure 15. SPPR wavelength shift as a function of silica-layer thickness around 92 ± 5 nm silver nanoparticles.

as novel properties can be acquired owing to the cooperative effects.[49] A recent report from this laboratory demonstrated a novel phenomenon, that is, light-induced coherent quadrupole coupling in self-assembled 2D arrays of $\approx$100 nm Ag nanoparticles.[50] The cooperative resonance of the assembly was characterized by an extremely sharp, nearly Lorentzian peak as compared to the SPPR of individual particles (Figure 16). This

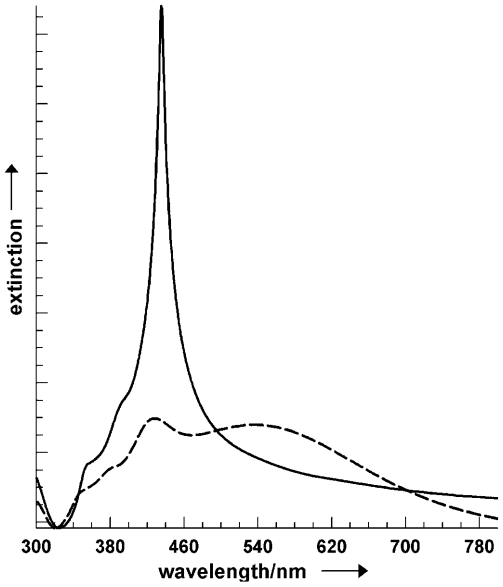

Figure 16. UV/Vis extinction spectra illustrating the difference between a suspension of non-interacting silver nanoparticles (-----) and a coupled, 2D array of silver nanoparticles (——).

resonance was measured as a function of interparticle spacing, which was controlled by biaxial stretching of arrays embedded into poly (dimethylsiloxane) (PDMS), as well as incident angle with linearly polarized light. As the interparticle spacing increased, the sharp peak rapidly decreased and the extinction spectrum evolved into the spectrum of non-interacting particles (Figure 17). The observed strong distance dependence indicated short-range, near-field coupling between the particles in the arrays. When closely-spaced particles are irradiated with light, their local EM fields overlap such that the only resonan-

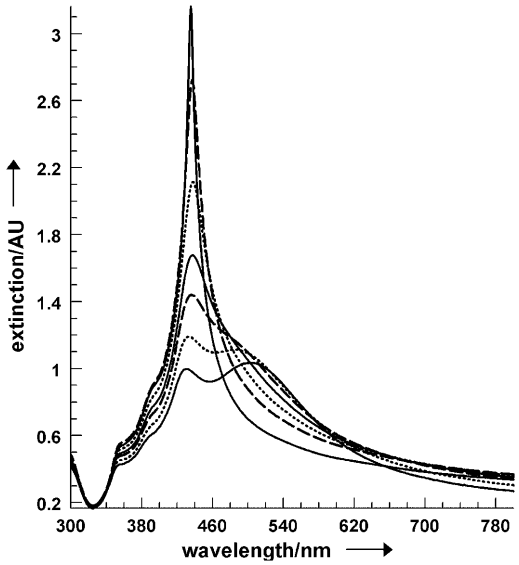

Figure 17. UV/Vis extinction spectra of a PDMS embedded silver nanoparticle array during biaxial stretching illustrating the decoupling of the resonance at increased interparticle distances.

ces that are supported are those for which the fields "constructively interfere". The fulfillment of this condition requires the electrons in adjacent particles to oscillate coherently, thereby making the coupling dependent upon the symmetry in arrays. In the case of a 2D array of Ag nanoparticles, the symmetry-allowed cooperative resonance is characterized by coherent quadrupolar oscillations of electrons in neighboring particles (Figure 18). The measured angular dependence further emphasized the coherent nature of the coupling as the cooperative resonance rapidly decreases with increasing incident angle. At oblique angles, the electrons in neighboring particles experience a slightly different phase of the incident wave that causes dephasing of the electron oscillations. When excited with p-polarized light, another peak appears in the red spectral range at small incident angles, indicating dipole coupling that is also damped due to dephasing at larger angles (Figure 19).

Other groups have noted a small blue-shift in the 2D assembly of 10 nm Ag particles and assigned it to dipolar coupling based on the fact that the dipole is the only visible SPPR of such small particles.[51] A particle of any diameter, however, can support electron oscillations of any shape (dipolar, quadrupolar, etc.) as determined by the symmetry conditions imposed by their neighbors. These considerations suggest that even small particles would exhibit quadrupolar coupling in 2D arrays, providing that the interparticle distance is sufficiently small.

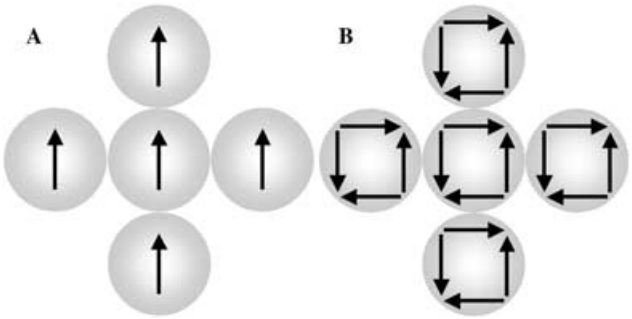

Figure 18. Schematic for A) dipolar and B) quadrupolar coupling between the SPPRs of individual silver nanoparticles in a 2D array. Arrows indicate the electric field lines of the resonance.

5. Summary and Outlook

For future practical applications of nanoparticles, synthesis techniques capable of producing highly crystalline metal particles of many different sizes and narrow size distribution are necessary. The hydrogen-reduction method discussed here fulfills these requirements for silver nanoparticles and perhaps other metals. Because of the chemical purity of the suspensions and the control that this method provides over particle size and distribution, the particles can be easily incorporated into a variety of nanocomposites and further assembled into higher-order nanostructures that exhibit novel properties.

Acknowledgements

We wish to thank Dr. Serhiy Malynych, Dr. Zhongchun Wang, Amar Kumbhar, J. Katrina Daniels, Mark Kinnan, Holly Robuck, Ryan White, and Catalina Cuervo for their contributions, the NSF, US EPA, and International SEMATECH for funding various aspects of this work, and Ames Laboratory for the equipment used in this work. We also acknowledge the Clemson University Center for Optical Materials Science and Engineering Technologies

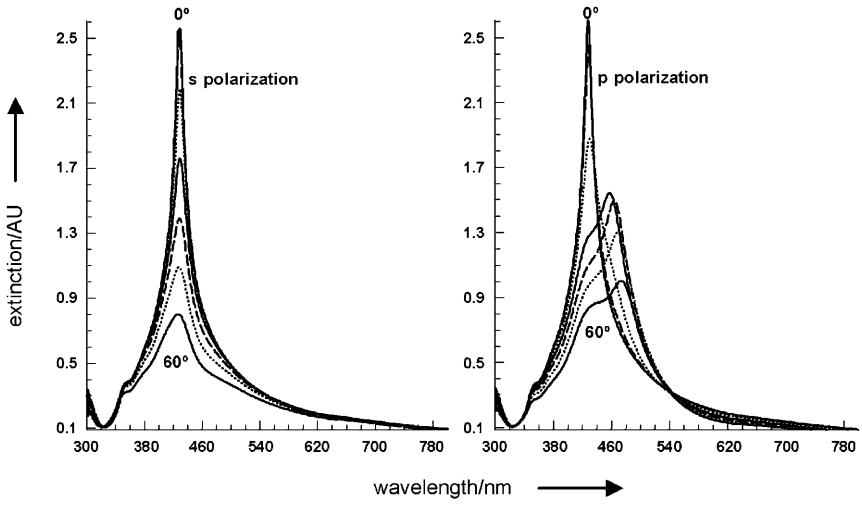

Figure 19. UV/Vis extinction spectra of 2D arrays of silver nanoparticles as a function of excitation incident angle using both s- and p-polarized light.

(COMSET) for continuous support and its members for helpful discussions.

Keywords: arrays · nanocomposites · nanoparticles · plasmon resonance · silver

[1] D. J. Barber, I. C. Freestone, *Archaeometry* **1990**, *32*, 33 – 45.
[2] M. Faraday, *Philos. Trans. R. Soc. London* **1857**, *147*, 145 – 181.
[3] a) J. J. Storhoff, R. Elghanian, C. A. Mirkin, R. L. Letsinger, *Langmuir* **2002**, *18*, 6666 – 6670; b) D. Roll, J. Malicka, I. Gryczynski, Z. Gryczynski, J. R. Lakowicz, *Anal. Chem.* **2003**, *75*, 3440 – 3445.
[4] G. Mie, *Ann. Physik IV* **1908**, *25*, 377 – 445; an English translation of this paper was provided by the British Library.
[5] M. Kerker, *The Scattering of Light and Other Electromagnetic Radiation*, Academic Press, Inc., New York, **1969**, pp. 54 – 63.
[6] P. Lilienfeld, *Appl. Opt.* **1991**, *30*, 4696 – 4698.
[7] M. Kerker, *Appl. Opt.* **1991**, *30*, 4699 – 4705.
[8] R. S. Shankland, "Electron", *Encyclopedia Americana*, Grolier Online, Feb. 1, **2005**, http://ea.grolier.com.
[9] J. Turkevich, P. C. Stevenson, J. Hillier, *Disc. Faraday Soc.* **1951**, *11*, 55 – 75.
[10] P. C. Lee, D. J. Meisel, *Phys. Chem.* **1982**, *86*, 3391 – 3395.
[11] J. A. Creighton, C. G. Blatchford, M. G. Albrecht, *J. Chem. Soc. Farad. Trans. II* **1979**, *75*, 790 – 798.
[12] a) R. W. J. Scott, H. Ye, R. R. Henriquez, R. M. Crooks, *Chem. Mater.* **2003**, *15*, 3873 – 3878; b) Y. Hou, S. Gao, *J. Mater. Chem.* **2003**, *13*, 1510 – 1512; c) A. Sinha, S. Kumar Das, T. V. Vijaya Kumar, V. Rao, P. Ramachandrarao1, *J. Mater. Synth. Proces.* **1999**, *7*, 373 – 377; d) M. Sastry, V. Patil, K. S. Mayya, D. V. Paranjape, P. Singh, S. R. Sainkar, *Thin Solid Films*, **1998**, *324*, 239 – 244.
[13] U. Kreibig, M. Vollmer, *Optical Properties of Metal Clusters*, Springer Series in Materials Science 25, New York, Springer-Verlag, **1995**, a) p. 50; b) p. 24; c) pp. 45–46; d) pp. 32–35; e) p. 13.
[14] a) D. D. Evanoff, Jr., G. Chumanov, *J. Phys. Chem. B* **2004**, *108*, 13957 – 13962; b) K. L. Kelly, E. Coronado, L. L. Zhao, G. C. Schatz, *J. Phys. Chem. B*, **2003**, *107*, 668 – 677.
[15] a) I. Sondi, D. V. Goia, E. Matijević, *J. Colloid Interface Sci.* **2003**, *260*, 75 – 81; b) J. P. Cason, K. Khambaswadkar, C. B. Roberts, *Ind. Eng. Chem. Res.* **2000**, *39*, 4749 – 4755; c) X. Li, J. Zhang, W. Xu, H. Jia, X. Wang, B. Yang, B. Zhao, B. Li, Y. Ozaki, *Langmuir* **2003**, *19*, 4285 – 4290; d) N. Shirtcliffe, U. Nickel, S. Schneider, *J. Colloid Interface Sci.* **1999**, *211*, 122 – 129; e) S. He, J. Yao, P. Jiang, D. Shi, H. Zhang, S. Xie, S. Pang, H. Gao, *Langmuir* **2001**, *17*, 1571 – 1575; f) N. Leopold, B. Lendl, *J. Phys. Chem. B* **2003**, *107*, 5723 – 5727; g) K. P. Velikov, G. E. Zegeres, A. van Blaaderen, *Langmuir* **2003**, *19*, 1384 – 1389; h) U. Nickel, A. Castell, K. Pöppl, N. Shirtcliffe, *Langmuir* **2000**, *16*, 9087 – 9091; i) Y. Tan, X. Dai, Y. Li, D. Zhu, *J. Mater. Chem.* **2003**, *13*, 1069 – 1075; j) R. He, X. Qian, J. Yin, Z. Zhu, *J. Mater. Chem.* **2002**, *12*, 3783 – 3786; k) D.-H. Chen, Y.-W. Huang, *J. Colloid Interface Sci.* **2002**, *255*, 299 – 302; l) K. K. Caswell, C. M. Bender, C. J. Murphy, *Nano Lett.* **2003**, *3*, 667 – 669; m) G. Rodríguez-Gattorno, D. Díaz, L. Rendón, G. O. Hernández-Segura, *J. Phys. Chem. B* **2002**, *106*, 2482 – 2487; n) D. L. Van Hyning, C. F. Zukoski, *Langmuir* **1998**, *14*, 7034 – 7046.
[16] a) M. Maillard, S. Giorgio, M.-P. Pileni, *J. Phys. Chem. B* **2003**, *107*, 2466 – 2470; b) S. Chen, D. L. Carroll, *Nano Letters* **2002**, *2*, 1003 – 1007.
[17] a) K. Esumi, A. Suzuki, A. Yamahira, K. Torigoe, *Langmuir* **2000**, *16*, 2604 – 2608; b) R. M. Crooks, M. Zhao, L. Sun, V. Chechik, L. K. Yeung, *Acc. Chem. Res.* **2001**, *34*, 181 – 190.
[18] a) Y. Sun, Y. Yin, B. T. Mayers, T. Herricks, Y. Xia, *Chem. Mater.* **2002**, *14*, 4736 – 4745; b) J. Zhang, B. Han, M. Liu, D. Liu, Z. Dong, J. Liu, D. Li, J. Wang, B. Dong, H. Zhao, L. Rong, *J. Phys. Chem. B* **2003**, *107*, 3679 – 3683.
[19] a) Y. Plyuto, J.-M. Berquier, C. Jacquiod, C. Ricolleau, *Chem. Commun.* **1999**, *17*, 1653 – 1654; b) T. C. Wang, M. F. Rubner, R. E. Cohen, *Langmuir* **2002**, *18*, 3370 – 3375.
[20] a) S. Z. Malynych, G. Chumanov, *J. Vac. Sci. Technol. A* **2003**, *21*, 723 – 727; b) Y.-P. Zhao, D.-X. Ye, G.-C. Wang, T.-M. Lu, *Nano Letters* **2002**, *2*, 351 – 354; c) T. R. Jensen, M. D. Malinsky, C. L. Haynes, R. P. Van Duyne, *J. Phys. Chem. B* **2000**, *104*, 10549 – 10556.
[21] F. Mafuné, J.-Y. Kohno, Y. Takeda, T. Kondow, H. Sawabe, *J. Phys. Chem. B* **2000**, *104*, 8333 – 8337.
[22] a) J. P. Abid, A. W. Wark, P. F. Brevet, H. H. Girault, *Chem. Commun.* **2002**, *7*, 792 – 793; b) H. H. Huang, X. P. Ni, G. L. Loy, C. H. Chew, K. L. Tan, F. C. Loh, J. F. Deng, G. Q. Xu, *Langmuir* **1996**, *12*, 909 – 912.
[23] a) N. A. Kotov, M. E. D. Zaniquelli, F. C. Meldrum, J. H. Fendler, *Langmuir* **1993**, *9*, 3710 – 3716; b) J. Zhu, S. Liu, O. Palchik, Y. Koltypin, A. Gedanken, *Langmuir* **2000**, *16*, 6396 – 6399.
[24] D. D. Evanoff, Jr., G. Chumanov, *J. Phys. Chem. B* **2004**, *108*, 13948 – 13956.
[25] A. Kumbhar, M. Kinnan, G. Chumanov, unpublished results.
[26] L. M. Liz-Marzán, M. Giersig, P. Mulvaney, *Langmuir*, **1996**, *12*, 4329 – 4335.
[27] W. Stöber, A. Fink, E. Bohn, *J. Colloid Interface Sci.* **1968**, *26*, 62 – 69.
[28] D. D. Evanoff, Jr., R. L. White, G. Chumanov, *J. Phys. Chem. B* **2004**, *108*, 1522 – 1524.
[29] A. Kumbhar, G. Chumanov, *J. Nanosci. Nanotech.* **2004**, *4*, 299 – 303.
[30] C. G. Granqvist, *Sol. Energy Mater. Sol. Cells*, **2000**, *60*, 201 – 262.
[31] Z. Wang, G. Chumanov, *Adv. Mater.* **2003**, *15*, 1285 – 1289.
[32] S. Malynych, I. Luzinov, G. Chumanov, *J. Phys. Chem. B*, **2002**, *106*, 1280 – 1285.
[33] S. Malynych, H. Robuck, G. Chumanov, *Nano Lett.* **2001**, *1*, 647 – 649.
[34] L. Quaroni, G. Chumanov, *J. Am. Chem. Soc.* **1999**, *121*, 10642 – 10643.
[35] a) Teflon is a registered trademark of Dupont; b) D. D. Evanoff, Jr., P. Zimmerman, G. Chumanov, *Adv. Mater.* **2005**, DOI: 10.1002/adma.200500391.
[36] a) H. Hiraoka, S. Lazare, *Appl. Surf. Sci.*, **1990**, *46*, 342 – 347; b) J. H. Lowry, J. S. Mendlowitz, N. S. Subramanian, *Opt. Eng.* **1992**, *31*, 1982 – 1985.
[37] a) R. Manor, A. Datta, L. Ahmad, M. Holtz, S. Gangopadhyay, T. Dallas, *IEEE Sensors J.* **2003**, *3*, 687 – 692; b) M. A. Kessler, E. A. H. Hall, *Thin Solid Films* **1996**, *272*, 161 – 169; c) G. G. Nenninger, P. Tobiška, J. Homola, S. S. Yee, *Sensors and Actuators B* **2001**, *74*, 145 – 151; d) R. P. Podgorsek, H. Franke, *Appl. Opt.* **2002**, *41*, 601 – 608.
[38] A. Biswas, O. C. Aktas, U. Schürmann, U. Saeed, V. Zaporojtchenko, F. Faupel, *App. Phys. Lett.* **2004**, *84*, 2655.
[39] A. J. Haes, W. P. Hall, L. Chang, W. L. Klein, R. P. Van Duyne, *Nano Lett.* **2004**, *4*, 1029 – 1034.
[40] R. A. R. Tricker, *Introduction to Meteorological Optics*, American Elsevier Publishing, New York, **1970**, pp. 225 – 229.
[41] P. B. Johnson, R. W. Christy, *Phys. Rev. B* **1972**, *6*, 4370 – 4379.
[42] A. Kawabata, R. Kubo, *J. Phys. Soc. Japan* **1966**, *21*, 1765 – 1772.
[43] N. W. Ashcroft, N. D. Mermin, *Solid State Physics*, Saunders College Publishing, Philadelphia, **1976**, pp. 2 – 20, 293 – 297, 347 – 348, 512 – 528.
[44] D. A. Weitz, T. J. Gramila, A. Z. Genack, J. I. Gersten, *Phy. Rev. Lett.* **1980**, *45*, 355 – 358.
[45] a) D. Steinmüller-Nethl, R. A. Höpfel, E. Gornik, A. Leitner, F. R. Aussenegg, *Phys. Rev. Lett.* **1992**, *68*, 389 – 392; b) B. Lamprecht, A. Leitner, F. R. Aussenegg, *Appl. Phys. B* **1999**, *68*, 419 – 423; c) Y.-H. Liau, A. N. Unterreiner, Q. Chang, N. F. Scherer, *J. Phys. Chem. B* **2001**, *105*, 2135 – 2142.
[46] B. J. Messinger, K. U. von Raben, R. K. Chang, P. W. Barber, *Phys. Rev. B* **1981**, *24*, 649 – 657.
[47] K. Kneipp, H. Kneipp, I. Itzkan, R. R. Dasari, M. S. Feld, *Chem. Rev.* **1999**, *99*, 2957 – 2975.
[48] A. J. Haes, S. Zou, G. C. Schatz, R. P. Van Duyne, *J. Phys. Chem. B* **2004**, *108*, 109 – 116.
[49] a) S. I. Stoeva, B. L. V. Prasad, S. Uma, P. K. Stoimenov, V. Zaikovski, C. M. Sorensen, K. J. Klabunde, *J. Phys. Chem. B* **2003**, *107*, 7441 – 7448; b) Q.-H. Wei, K.-H. Su, S. Durant, X. Zhang, *Nano Lett.* **2004**, *4*, 1067 – 1071; c) C. D. Jones L. A. Lyon, *J. Am. Chem. Soc.* **2003**, *125*, 460 – 465.
[50] S. Malynych, G. Chumanov, *J. Am. Chem. Soc.* **2003**, *125*, 2896 – 2898.
[51] M. N. Dulin, *Z. Phys. D* **1993**, *26*, 172 – 174.

Received: February 23, 2005
Published online on June 8, 2005

